A novel xenograft model reveals invasive mesenchymal transition and ineffective angiogenic response during the evolution of resistance to anti-angiogenic therapy

By Arman Jahangiri,[1‡] William Chen,[1‡] Ankush Chandra,[1] Alan Nguyen,[1] Jacob Weiss,[1] Kayla J. Wolf,[2] Jung-Ming G. Lin,[2] Jonathan Rick,[1] Maxim Sidorov,[1] Patrick Flanigan,[1] Garima Yagnik,[1] W. Shawn Carbonell,[3] Sanjay Kumar,[2] Manish K. Aghi[1]

[1]Dept. of Neurosurgery; University of California San Francisco (UCSF); [2]Dept. of Bioengineering; University of California Berkeley; and [3]Oncosynergy Inc.; San Francisco, CA

Correspondence to: Manish K. Aghi, MD, PhD; Professor of Neurological Surgery; UCSF; Diller Cancer Research Building; 1450 Third Street Room HD-465; San Francisco, CA 94158; 415-353-3907 FAX; 415-353-1172

Keywords: bevacizumab, glioblastoma, mesenchymal, invasion, xenograft

Running title: Mesenchymal change during anti-angiogenic therapy resistance

The authors disclose no potential conflicts of interest

[‡]Authors contributed equally to this work

ABSTRACT

Bevacizumab treatment of glioblastoma is limited by transient responses and acquired resistance. Because of the lengthy duration of treatment that can precede resistance in patients, in order to study changes underlying the evolution of bevacizumab resistance, we created a novel multigenerational xenograft model of acquired bevacizumab resistance. Glioblastoma xenografts were treated with bevacizumab or IgG, and the fastest growing tumor reimplanted into new mice, generating paired isogeneic responsive or resistant multigenerational xenografts. Microarray analysis revealed significant overexpression across generations of the mesenchymal subtype gene signature, paralleling results from patient bevacizumab-resistant gliobalstomas (BRGs) that exhibited increasing mesenchymal gene expression correlating with increased bevacizumab treatment duration. Key mesenchymal markers, including YKL-40, CD44, SERPINE1, and TIMP1 were upregulated across generations, with altered morphology, increased invasiveness, and increased neurosphere formation confirmed in later xenograft generations. Interestingly, YKL-40 levels were elevated in serum of patients with bevacizumab-resistant vs. bevacizumab-naïve glioblastomas (52.4 vs. 24.2 ng/mL; $P<0.05$). Finally, despite upregulation of VEGF-independent pro-angiogenic genes across xenograft generations, immunostaining revealed increased hypoxia and decreased vessel density with increasing generation of treatment, mirroring our findings in patient BRGs and suggesting tumor growth despite effective devascularization caused by VEGF blockade. Besides identifying novel targets for preventing the evolution of resistance and offering a xenograft model for testing resistance inhibitors,

our work suggests YKL-40 as a blood biomarker of bevacizumab resistance worthy of further evaluation.

INTRODUCTION

The premise that the angiogenic switch is critical to malignant tumor progression has been validated by preclinical[21] and clinical[13] studies showing the efficacy of angiogenesis inhibitors. Most angiogenesis inhibitors target vascular endothelial growth factor (VEGF) due to its key role in angiogenesis. Based on encouraging clinical trial results,[15] humanized anti-VEGF antibody bevacizumab is approved as monotherapy for recurrent glioblastoma (GBM). Unfortunately, bevacizumab responses are typically transient, with 50% of GBMs [15] that initially respond progressing soon thereafter, with acquired bevacizumab resistance associated with poor outcomes.[6] Indeed, phase III trials of bevacizumab in newly diagnosed[5, 10] and recurrent GBM revealed increased progression free survival (PFS) but no impact on overall survival (OS).

While some studies have suggested that resistance to anti-angiogenic therapy is associated with upregulation of compensatory VEGF-independent angiogenesis, others have suggested that resistance involves mesenchymal gene expression changes driving perivascular invasiveness along the remaining blood vessels in an otherwise successfully devascularized tumor.[12, 21] Furthermore, while xenograft studies have suggested that a short course of tumor treatment with anti-VEGF antibody promotes some degree of mesenchymal transition,[3, 20] the impact of duration of treatment, which can be far more prolonged in patients than in xenografts, has yet to be investigated in patients. We hypothesized that the full resistant phenotype emerges gradually over a prolonged course of treatment and involves mesenchymal gene expression changes driving perivascular invasiveness. We investigated this hypothesis in specimens from

patients whose tumors progressed after variable duration of bevacizumab treatment and by creating a novel multi-generational xenograft model of bevacizumab resistance.

RESULTS

To define endpoints for the evolution of bevacizumab resistance that would guide the development of a multi-generational xenograft model, we investigated the impact of bevacizumab-treatment duration on the phenotype of patient bevacizumab-resistant glioblastomas (BRGs). Immunohistochemistry for hypoxia marker CA9 revealed that BRG hypoxia increased with increasing duration of bevacizumab treatment before progression (**Fig. 1a**; P=0.004), while vessel density, assessed by CD31 staining, decreased (**Fig. 1b**; P=0.04), and Ki-67 labeling did not change (**Fig. 1c**; P=0.6). We then used our previously published microarray analysis of 15 bevacizumab-resistant glioblastomas relative to paired pre-treatment glioblastomas from the same patients [8, 11] to analyze expression of the genes previously used to define three glioblastoma subtypes (proneural, mesenchymal, and proliferative).[19] This analysis revealed a significant tendency for tumors to become more mesenchymal and less proneural with increasing duration of bevacizumab treatment before progression (**Fig. 1d**; P=0.01).

To further define changes associated with the evolution of bevacizumab resistance, we established a novel xenograft model of anti-angiogenic therapy resistance.[4, 11] Because acquired anti-angiogenic therapy resistance arises after prolonged treatment, U87 xenografts were treated with bevacizumab or IgG during serial *in vivo* subcutaneous passaging for 9 generations, with the most resistant xenograft selected for repropagation each generation, creating 9 generations of U87-

Bev^R and U87-Bev^S xenografts, whose bevacizumab-resistance versus responsiveness, respectively, were confirmed in subcutaneous and intracranial microenvironments (**Fig. 2A**).[4, 11] The ability of the model to replicate human bevacizumab-resistant glioblastomas and the necessity of multiple generations of treatment to model patient resistance was confirmed because four key features in bevacizumab-resistant glioblastomas[6, 8] appeared in the xenograft model but did not culminate until the fifth generation of U87-Bev^R. First, resistance rate, the frequency of tumors reaching volumetric endpoint by 45 days, rose from 13% to 100% during the first 5 generations (**Fig. 2b; Supplementary Figs. S1-3**). Second, tumor growth rate increased with each U87-Bev^R generation until surpassing that of U87-Bev^S by the fifth generation (**Fig. 2c; Supplementary Figs. S1-3**). Third, the tumors exhibited decreased vessel density (**Fig. 2d**) and increased hypoxia (**Fig. 2e**) with increasing generation of treatment. Fourth, Ki67-labeling did not change with each generation of treatment (**Fig. 2f**). Thus, like patient BRGs, our multi-generational xenograft model exhibited increased hypoxia with decreased vessel density with increasing duration of bevacizumab treatment, suggesting that bevacizumab-resistant glioblastomas grow despite successful bevacizumab-induced devascularization.

To serially investigate transcriptional changes associated with the evolution of bevacizumab resistance, we performed microarray expression analysis of U87-Bev^R generations 1, 4, and 9, with generation four of U87-Bev^R chosen because of the dramatic increase in tumor growth rate that occurred during this generation (**Fig. 2c**). Gene set enrichment and ontology analysis revealed significant upregulation across U87-Bev^R generations 4 (**Fig. 3a**) and 9 (**Fig. 3b**) of genes involved in metabolism,

angiogenesis, and inflammatory response, and downregulation of genes involved in DNA packaging and translation, chromatin assembly, and mitosis.

To determine if our multigenerational xenograft model replicated the mesenchymal gene expression changes we noted in bevacizumab-resistant patient glioblastomas, we investigated the set of U87-Bev^{R} genes significantly dysregulated across xenograft generations, finding that mesenchymal genes were significantly over-represented and upregulated, while proneural genes were significantly under-represented and downregulated (**Fig. 4a-b**). To validate these findings, we performed qPCR for 14 genes in our array that were also part of a previously described mesenchymal gene set in GBM[19] and found increased expression in all but one gene by generation 9 (**Fig. 4c**). To integrate and elaborate upon these findings, we averaged the expression of these 14 mesenchymal genes by qPCR, along with the 15 proneural and 5 proliferative genes described in the same study[19] that were also part of our microarray to obtain mesenchymal, proneural, and proliferative gene expression scores on a +1 to -1 scale. Doing so revealed increased mesenchymal gene expression approaching +1 by generation 4 and persisting thereafter (**Fig. 4d**), mirroring mesenchymal gene expression changes which occurred with increasing duration of bevacizumab treatment in patient BRGs. Finally, to determine if the secretion of any of these factors in the setting of bevacizumab resistance was high enough to elevate them in the serum and serve as a potential biomarker of this bevacizumab-induced mesenchymal change, we investigated levels of YKL-40 in the serum of patients with BRGs (n=8) versus bevacizumab-naïve GBMs (n=11), finding significantly elevated

serum levels of YKL-40 in BRG patient serum compared to serum from recurrent bevacizumab-naïve GBMs ($P<0.05$; **Fig. 4e**).

Because our microarray analysis revealed multiple dysregulated genes implicated in cytoskeletal and extracellular matrix re-organization and regulation of tumor cell migration and invasion, including increased expression of RHOQ and RHOE, FYN, FGD3, TIMP1, SERPINE1, HBEGF, DUSP1 as well as decreased expression of a tumor motility suppressor, DPYSL3 (**Fig. 5a**), we then investigated if these mesenchymal and invasive gene expression changes noted in U87-Bev^R were associated with the altered morphology and increased invasiveness that we have previously described in BRGs[4, 6, 8, 11] and that have been described for mesenchymal cancers in general. U87-Bev^R cells exhibited more stellate morphology ($P<0.01$; **Fig. 5b-c**) and increased invasiveness in Matrigel assays compared to U87-Bev^S cells ($P=0.003$-0.04; **Fig. 5d; Supplementary Fig. S4**). We then further investigated the invasive potential of U87-Bev^R and U87-Bev^S cells in three-dimensional bioengineered hydrogel and microchannel platforms that modeled white matter tracts (**Fig. 5e**) and perivascular invasion (**Fig. 5f; Supplementary Figs. S5-6**), respectively, and found that U87-Bev^R cells were more invasive in both contexts ($P<0.05$).

Our transcriptional analysis also identified significantly dysregulated genes previously shown to be markers of or to be involved in regulation of glioma stem cells, including CD44, LIF, IL6, and ZEB1, leading us to investigate if patient BRGs exhibited enrichment of a tumor stem cell population. Prospective plating of cells from patient BRGs vs. bevacizumab-naïve glioblastomas (n=3/group) in neurosphere medium revealed significantly increased cell counts from dissociated neurospheres in BRGs

compared to bevacizumab-naïve GBMs (**Fig. 6a**; P<0.001). Although U87-Bev^R cells formed fewer neurospheres than U87-Bev^S cells, U87-Bev^R neurospheres were larger (p=0.002) and markedly more cellular (p=0.0002) as compared to U87-Bev^S cells (**Fig. 6b-f**). To investigate potential mediators of the stemness and mesenchymal change identified in U87-Bev^R xenografts and BRGs, qPCR was performed on explanted U87-Bev^R and U87-Bev^S tumors for GLUT3 and ZEB1, genes associated with both properties.[9, 17] U87-Bev^R xenografts exhibited increased GLUT3 and ZEB1 gene expression (P=1X10^{-5}-0.02; **Fig. 6g**).

Interestingly, our microarray analysis also revealed expression changes in angiogenesis pathways, suggesting that anti-angiogenic therapy triggered attempted compensatory upregulation of non-VEGF angiogenic pathways, with increased expression of 30 angiogenesis-related genes, sometime as early as generation 1 and peaking in generation 4 of U87-Bev^R relative to U87-Bev^S (**Fig. 7a**). These findings were validated by qPCR for these 30 genes, revealing a peak occurring at generation 4 of U87-Bev^R relative to U87-BevS (**Figs. 7b-c**). Among these upregulated genes were several secreted pro-angiogenic factors, including GREM1, FGF2, YKL-40, WNT5A, IL6, IL1A, and IL1B (**Fig. 7d**). However, our immunostaining of xenografts and patient specimens would suggest that this upregulation of genes mediating VEGF-independent angiogenesis failed to meaningfully impact tumor vascularity, based on the reduced vessel density and increased hypoxia noted with increasing treatment duration in resistant patient glioblastomas and xenografts. To determine if this ineffectiveness reflected the upregulated secreted angiogenic genes in U87-Bev^R failing to achieve biologically meaningful levels, we analyzed the effect of conditioned media (CM) from

cultured U87-Bev^R and U87-Bev^S cells on the formation of endothelial tubules in HUVEC cells. We found that U87-Bev^R CM drove increased endothelial segment and mesh formation compared to U87-Bev^S conditioned media (P=0.0007-0.01) and that, while bevacizumab blocked U87-Bev^S effects on HUVEC cells (P=0.0004), by generation nine, bevacizumab failed to block the increased U87-Bev^R effects on HUVEC cells (**Fig. 7e; Supplementary Fig. S7**). While the angiogenic factors secreted by U87-Bev^R cells could cause an effective VEGF-independent angiogenic response in culture, the hypovascularity and hypoxia of U87-Bev^R and BRGs could reflect additional *in vivo* effects rendering this compensatory angiogenic response ineffective in the setting of prolonged bevacizumab treatment.

DISCUSSION

The failure of anti-angiogenic agents like bevacizumab to achieve durable response in glioblastoma[5] and other cancers[18] has led to studies investigating the genetic reprogramming occurring in these tumors. Xenograft studies have suggested that tumor treatment with anti-VEGF antibody until tumor growth meets euthanasia criteria promotes increased transcription of mesenchymal factors that portend a worse prognosis in glioblastoma and other cancers.[3, 20] However, this approach may not fully model patient resistance because it fails to replicate the duration of treatment patients receive, which can be far more prolonged than the duration of treatment that a xenograft receives before meeting euthanasia criteria. We sought to define the impact of prolonged duration of bevacizumab treatment on the genetic reprogramming of

glioblastoma using our novel multi-generational xenograft model of bevacizumab resistance. The impact of this multi-generational approach was underscored by our finding that resistance did not become entrenched and irreversible until the fourth generation, the time at which the gene expression and functional changes associated with resistance peaked, suggesting that previous studies treating a single xenograft generation until euthanasia may not be using an adequate endpoint to model resistance to anti-angiogenic therapy.

Among the findings emerging from patient specimens and replicated from our xenograft model were the hypoxia and devascularization seen in BRGs, indicating that the resistance occurs despite continued successful devascularization caused by bevacizumab. Indeed, this devascularization succeeds despite upregulation of compensatory VEGF-independent pro-angiogenic pathways and despite enriched neurosphere yield and expression of genes associated with the stem cells shown to be capable of forming endothelial cells[23] in bevacizumab-resistant xenografts.

Prognostic classification schemes have been created to designate molecular subtypes of glioblastomas based on similarity to defined expression signatures. Of the existing classification schemes, in order to study subtype changes associated with bevacizumab resistance, we chose to use that of Phillips et al.,[19] which uses more focused gene sets to define subtypes that change during glioblastoma evolution, in contrast to other classification schemes like that of Verhaak et al. which uses more extensive gene sets to define glioblastoma subtypes that do not change during tumor evolution.[22] Using this classification scheme, we demonstrated mesenchymal change in our multigenerational xenograft model, mirroring our finding in BRGs. We found that this

mesenchymal change had an associated biomarker, elevated serum YKL-40 in BRG patients. Similarly, serum YKL-40 elevation during bevacizumab treatment of ovarian cancer patients has been described as a predictor of shorter PFS with low baseline YKL-40 associated with improved outcomes.[2]

Besides providing insight into potential biomarkers of bevacizumab resistance, our xenograft model could also offer insight into the optimal upstream regulators of bevacizumab resistance to target in order to prevent the evolution of this resistance before it becomes entrenched. Because bevacizumab resistance has been challenging to pharmacologically target,[24] these insights and the ability to screen inhibitors of bevacizumab resistance in our model could provide meaningful benefit to glioblastoma patients.

MATERIALS AND METHODS

Cell Culture

HUVEC cells (ATCC) were passaged fewer than 6 times, and confirmed to be Mycoplasma-free and verified by providing companies using short tandem repeat (STR) profiling. Cells for culture were obtained from U87-Bev^{R} and U87-Bev^{S} xenografts generated as described.[4, 11] Cells were cultured in DMEM/F-12 supplemented with 10% FBS and 1% P/S and maintained at 37°C. U87-Bev^{S}, U87-Bev^{R} and primary GBM neurospheres were cultured in Neurocult/Neurosphere media (StemCell Technologies) with 10 ng/ml bFGF (Thermo Fisher), 20 ng/ml EGF (Thermo Fisher) and B27 and N2 supplement (Thermo Fisher) and maintained at 37°C. Accutase (StemCell Technologies) was used to dissociate neurospheres into a single cell suspension.

Morphology Analysis

U87-Bev^S and U87-Bev^R (generations 1,4 and 9) were plated in a chamber slide system (Thermo Fisher) under normal cell culture conditions for 24 hours. Once adhered to the chamber slides, cells were fixed in 4% paraformaldehyde for 30 minutes, then washed three times with PBS after which cells were incubated in Phalloidin stain (1:200 in TNB; Sigma) for one hour at room temperature and washed again three times with PBS. Lastly, chamber slides were mounted with DAPI-Fluoromount G (Southern Biotech, 0100-20, Birmingham, AL, USA) and coverslipped. Slides were imaged using a Zeiss AxioObserver Z1 system equipped with an AxioCam MRm CCD and AxioVision software (Release 4.8). Cell morphology was quantified by calculating Form Factor [4πx area/√(perimeter)] using the Shape Descriptor plugin in ImageJ (NIH).

Generation of Neurospheres and Functional Assays

Neurospheres were generated from patient GBM tumor by dissociating tumor chunks into a single cell suspension in full Neurocult media at a density of 100,000 cells. U87-Bev^S and U87-Bev^R neurospheres were generated by seeding the respective cell lines at 50,000, 100,000 and 200,000 cells in neurosphere media. Neurospheres were isolated and stained for cancer stem cell markers (CD133 and Nestin) as described by Kim et al.[14] to confirm stem cell isolation. Neurosphere reformation assay, diameter quantification and total cell counts were done by seeding 100,000 cancer stem cells in neurosphere media. At the end of 7 days, tile imaging was performed using a Zeiss

AxioObserver Z1 system from which number of spheres and diameters were calculated. Single cell suspensions were prepared from the neurospheres to get absolute cell counts from patient GBM neurospheres as well as U87-BevS and BevR cell lines.

Microarray Analysis

Tumor chunks previously harvested from generational xenografts had been flash frozen at explantation and stored in liquid nitrogen. Samples for the microarray analysis were retrieved from storage and dissociated using both a QiaShredder (Qiagen) and passage through a 21-gauge sterile syringe. Dissociated tissue was then processed to obtain RNA using the RNeasy kit (Qiagen), following standard manufacturer's protocol. RNA was tested for quality using an RNA 6000 chip with the Bioanlyzer hardware (Agilent). RIN scores of greater than 8 were required to ensure RNA quality. RNA was then converted to labeled cRNA using the TargetAmp-Nano Labelling Kit for Illumina Expression BeadChip (EpiCentre), following standard manufacturer's protocol. Labelled cRNA was kept at -20°C and given to the UCSF Genome Core Facility (GCF) for chip hybridization.

Bioinformatics

Data (.idat files) from GCF analysis of our xenograft arrays underwent standard QC and processing through the UCSF Bioinformatics Core, and were deposited in GEO (Accession number=GSE81465). In parallel, we accessed our previously archived[8] microarray analysis of BRGs and their paired pre-treatment GBMs deposited in ArrayExpress (accession no. E-MEXP-3296). Gene set enrichment analysis was

performed in R using the GAGE package (v2.28.2). A pre-existing set 1000 gene ontology (GO) gene lists within the GAGE package was used to identify enriched gene ontologies in the positive (upregulated) and negative (downregulated) directions. To identify significantly dysregulated genes across generations, a two-component normal mixture-model was fitted by expectation-maximization to the Z-transformed Log(variance) distribution of gene expression values over generations 4 and 9. A posterior probability cutoff of ≥0.95 was applied, resulting in 717 significantly dysregulated genes. Next, a non-parametric bootstrap procedure was used to determine over-representation of the Philips et al mesenchymal, proneural, and proliferative gene sets among these dysregulated genes. Microarray probes were mapped to HGNC gene names, and uniform random sampling of 717 of the 48,324 gene probes, including duplicate probes, and matching to the mesenchymal, proneural, or proliferative gene set was repeated 50,000 times, resulting in a putative null distribution of the number of matches to the gene set in question. A Poisson probability density function was fit by maximum likelihood estimation (MLE) to this distribution and a 1-tailed p-value calculated for the observed number of matches to the gene set in question. Genes were further clustered by k-means clustering based on gene expression trajectory across generations, and these expression trajectory clusters were manually curated into sets of upregulated genes (sustained increases in expression through generation 4 and 9), downregulated genes (sustained decreases in expression through generation 4 and 9), and other genes. Finally, expression of particular genes of interest identified from microarray analysis were validated using qPCR.

Quantitative PCR

After obtaining RNA from xenografts as described in the microarray analysis, cDNA was created using qScript XLT cDNA Supermix (Quanta Bio), both following standard manufacturer's protocol. cDNA was diluted to a constant concentration for all samples to ensure similar nucleic acid loading levels. Quantitative PCR was carried out using Power Syber Green Master Mix (Applied Biosystems). Primer sequences can be found in **Supplementary Tables S1-S2**. qPCR was performed on an Applied Biosystems StepOne Real-Time PCR cycler following recommended guidelines described by Applied Biosystems for Syber: 95° C for 10 min, followed by 40 cycles of 95° C for 15 sec and 60° C for 1 min. Ct values were calculated using the StepOne software accompanying the real-time cycler. Samples were prepared with three technical replicates for each primer pair and used ACTB as a control housekeeping gene.

Human Serum ELISA

GBM patient serum was obtained through the UCSF Brain Tumor tissue bank which, through an IRB-approved protocol (10-01318), obtained tissue after informed consent from patients. YKL-40 ELISAs (R&D Systems) were performed in triplicate on serums diluted 1:50.

Microchannel Device Fabrication

The microchannel device was fabricated as described by Lin et al.[16] Briefly, the micropatterned polyacrylamide (PA) gel (8%T, 3.3%C acrylamide/bisacrylamide

(Sigma-Aldrich) was activated with Sulfo-SANPAH (Thermo Scientific) and incubated with a 1:2 dilution of Matrigel (Fisher Scientific, Cat# CB40230, diluted in 10% FBS cell culture medium) for 24 hours at 4°C (see **Supplementary Methods**). The micropatterned PA gel was then incubated in 0% FBS cell culture medium at 37°C for at least 1 hour prior to device fabrication. Following incubation, the gel was removed and the excess liquid was aspirated away. The PDMS lid was gently placed on top of the PA gel (see **Supplementary Methods**), with the holes in the PDMS aligned to the inlet and outlet microwell patterns on the PA gel. The hybrid PDMS/PA device was then placed under vacuum (200 mmHg) in a vacuum desiccator (Bel-Art) for 6 minutes to reversibly seal the layers together. After the vacuum step, 0% FBS cell culture media was place in both inlet ports and allowed to equilibrate in the device. To seed the device, any excess medium was first aspirated from all four inlet and outlet ports. Then a 30 µl aliquot of cell suspension (1 million cells per mL) was added to the top inlet port. Due to the pressure differences, cells flow into and lodge at the start of the migratory microchannels. The cells were then allowed to adhere for one hour prior to chemokine gradient formation and imaging, with 20 ng/ml SDF-1 (R&D Systems) diluted in 10% FBS used as the chemokine.

Cell Motility Measurements in Microchannel Device

Live-cell imaging was performed using a Nikon Ti-E2000-E2 microscope equipped with a motorized, programmable stage (Applied Scientific Instrumentation), an incubator chamber to maintain constant temperature, humidity, and CO2 levels (In vivo Scientific), a digital camera (Photometrics CoolSNAP HG II), and NIS Elements (Nikon Instruments

Inc.) software. Images were taken at 5 ms exposure, 2x2 pixel binning using a 10x-objective (Nikon CFI Plan Fluor DLL 10x). We measured cellular motility using 10X phase contrast time-lapse images acquired every 15 minutes over a 3-hour period. ImageJ software (NIH) was used to track the centroid of each cell from one frame to another to yield instantaneous migration speeds, which were then averaged over the entire time course of the experiment to yield the migration speed of a cell. Cells that were observed to be sticking to each other were also excluded from analysis.

HA Matrix Synthesis

HA hydrogels were synthesized as previously described.[1] Briefly, sodium hyaluronate (Lifecore Biomedical, Research Grade, 66 kDa - 99 kDa) was functionalized with methacrylate groups (Me-HA) using methacrylic anhydride (Sigma-Aldrich, 94%). The extent of methacrylation per disaccharide was quantified by ^{1}H NMR as detailed previously and found to be ~85% for materials used in this study. To add integrin-adhesive functionality, Me-HA was conjugated via Michael Addition with the cysteine-containing RGD peptide Ac-GCGYGRGDSPG-NH2 (Anaspec) at a concentration of 0.5 mmol/L. Finally, 3wt% Me-HA was crosslinked in phenol-free DMEM (Invitrogen) with bifunctional thiol dithiothretiol (DTT, Sigma-Aldrich). After 1 hr of crosslinking, the hydrogels were rinsed and soaked in room temperature PBS for 1 hr before cell seeding. The shear modulus of hydrogel formulations was measured using oscillatory rheometry (Anton Parr Physica MCR 310) as described previously.[25] Briefly, hydrogels were first crosslinked by incubation for 1 hr in a humidified 37˚C chamber. Rheological testing consisted of frequency sweeps ranging from 100 to 0.1 Hz at 0.5% amplitude

also in a humidified 37˚C chamber. Shear modulus was reported as the average storage modulus for 3 tests per type of matrix composition at an oscillation frequency of 0.5 Hz. A concentration of 19 mmol/L DTT was selected to yield a shear modulus of ~300 kPa for all studies.

HA Invasion Device Fabrication

Device fabrication will be described in detail in a forthcoming manuscript. Briefly, the PDMS PDMS (Sylgard 184 elastomer) supports for hydrogels were fabricated by molding PDMS to have two open channels (~170 µm in diameter) in parallel with ~500 µm spacing between channels. A gap was cut into the PDMS allowing space for gel casting. To cast the gel, wires were first reinserted into the assembled device to create a mold. Next, the hydrogel matrix was inserted in the side of the device. Wires were removed after the hydrogel solution had solidified leaving two open channels. After rinsing and soaking the hydrogels, cells were inserted into the freshly fabricated device using a syringe (Hamilton). Cut wires were used to plug each end of the cell reservoir, and the entire device was placed into the bottom of a 6-well plate and bathed in 3 mL of medium. Cells and gels were equilibrated in medium overnight before imaging. Medium was changed every 3 days.

Invasion and Protrusion Analysis

For area analysis in HA Invasion devices, cells in devices were imaged once every 3 days using Eclipse TE2000 Nikon Microscope with a Plan Fluor Ph1 10x objective.

Images were acquired and large images were stitched using NIS-Elements Software. For each device, the total cell area was outlined in ImageJ and normalized to the total cell area from day 1. To analyze morphology, protrusions visible at the edge of the invading mass of cells were counted and normalized to the length of the cell mass. Each device was fabricated and seeded independently. GraphPad Prism 7 software was used to graph data and perform statistical analysis. Data was compared using ANOVA followed by Tukey Kramer multiple comparisons test (n=3-4 independent devices per condition).

Blood Vessel Formation Assay

HUVEC cells were grown on matrigel in HUVEC media with or without 100 ng/mL bevacizumab. U87-Bev^{R} or U87-Bev^{S} cells from variable generations were grown in DMEM/10% FBS in overlying Boyden chambers. Cells were imaged every 4 hours for 20 hours. An ImageJ plug in was used to compute number of mesh and vessel segments, as described previously.[7]

Statistics

The student's t-test and Mann-Whitney tests were used to compare means of continuous parametric and non-parametric variables, respectively. Paired t-tests (parametric) and Wilcoxon signed-rank tests (non-parametric) were used to compare pre- and post-treatment variables from the same patients. Interobserver variability for manual counting of immunofluorescence was assessed using SPSS VARCOMP analysis. P values are two-tailed and $P<0.05$ was considered significant.

CONFLICT OF INTEREST

The authors report no competing financial interests in relation to the work described.

ACKNOWLEDGEMENTS

M.K.A. was supported by the American Brain Tumor Association (ABTA), the James S. McDonnell Foundation, American Cancer Society (ACS), University of California Cancer Research Coordinating Committee, and the NIH (5K02NS64167 and 1R01NS079697). A.J., A.C., and J.R. were supported by Howard Hughes Medical Institute (HHMI) fellowships. W.C. and J.R. were supported by UCSF School of Medicine (SOM) Pathways Explore Summer Grants. K. J. W. was sponsored by an NSF Predoctoral Fellowship. S.K. was sponsored by the NIH (1R21CA174573, 1R01GM122375, 1R21EB025017).

FIGURE LEGENDS

Figure 1. Increasing treatment duration drives hypoxia and mesenchymal gene expression in patient bevacizumab-resistant glioblastoma. (**a**) increased CA9 staining, (**b**) decreased vessel density, (**c**) unchanged proliferation, and (**d**) increased mesenchymal / decreased proneural gene expression were seen with increased duration of bevacizumab treatment in patient bevacizumab-resistant glioblastomas.

Figure 2. A multi-generational xenograft model replicates the phenotype and gene expression of patient bevacizumab-resistant glioblastoma. (**a**) Schema of the approach used to create the multi-generational bevacizumab-resistant xenograft model (**b**) The percentage of tumors that were resistant to bevacizumab increased with each U87-Bev^R generation. (**c**) U87-Bev^R tumor growth rate increased with each generation. (**d**) Decreased vessel density was noted with increasing generation of U87-Bev^R. (**e**) increased hypoxia density was noted with increasing generation of U87-Bev^R. (**f**) MIB-1 labeling did not change with each generation of U87-Bev^R.

Figure 3. Significantly altered gene ontologies during evolution of bevacizumab resistance in a multi-generational xenograft model. GAGE gene set enrichment analysis revealed enrichment and upregulation of gene ontologies associated with metabolism, angiogenesis, and inflammatory response, and downregulation of genes involved in DNA packaging and translation, chromatin assembly, and mitosis. The top ten enriched gene ontologies are displayed.

Figure 4. A multi-generational xenograft model replicates the mesenchymal gene expression of bevacizumab-resistant glioblastoma. (**a-b**) Bootstrapping analysis revealed the Philips et al mesenchymal gene set to be highly over-represented and proneural gene set to be under-represented among genes significantly dysregulated across U87-Bev^R generations, with 19 of 170 (11%) mesenchymal genes and 9 of 338 (2%) proneural genes found to be dysregulated. 37% of mesenchymal genes were upregulated, while 44% of proneural genes were downregulated. (**c**) Increased expression of signature mesenchymal genes was confirmed by qPCR, with marked upregulation of the secreted factor, YKL-40. (**d**) Expression of signature mesenchymal, proneural, and proliferative genes were normalized and plotted on a -1 to +1 scale, revealing the evolutionary trajectory of transcriptional subtypes across U87-Bev^R generations, with increased mesenchymal gene expression approaching +1 by generation 4 and persisting thereafter. (**e**) ELISA reveals elevated YKL-40 levels in patients with GBMs resistant to bevacizumab compared to patients with recurrent bevacizumab-naïve GBM and healthy donors *, $p<0.05$, **, $p<0.01$, ***, $p<0.001$

Figure 5. A multi-generational xenograft model replicates the invasiveness of patient bevacizumab-resistant glioblastomas. (**a**) Microarray analysis revealed dysregulation of multiple genes in U87-Bev^R (versus U87-Bev^S) associated with cytoskeletal and extracellular matrix re-organization, migration, and invasion. (**b**) Immunofluorescent imaging of cells from generations 1,4 and 9 of U87-Bev^R with Phalloidin reveals cellular morphology. (**c**) Morphological analysis of generations 1,4 and 9 of U87-Bev^R reveals lower form factor associated with generations 4 and 9 of

U87-Bev^R. (**d**) Matrigel invasion assay reveals a higher invasiveness of multiple generations of U87-Bev^R when compared to U87-Bev^S. (**e**) 3D bioengineered hydrogel assay modeling white matter tracts and (**f**) 3D bioengineered microchannel platform modeling perivascular invasion through hyaluronic acid (HA) matrix reveal a higher invasiveness ($P<0.001$ hydrogel and $P<0.05$ microchannel) of multiple generations of U87-Bev^R compared to U87-Bev^S cells. *, $p<0.05$, **, $p<0.01$, ***, $p<0.001$. Scale bar= 50μm

Figure 6. A multi-generational xenograft model replicates the stem cell-enrichment of bevacizumab-resistant glioblastomas. (**a**) Higher total stem cell count yield from neurospheres derived from bevacizumab-resistant patient tumors when compared to bevacizumab-naïve patient tumors ($p<0.001$). (**b**) Immunofluorescent staining of neurospheres derived from U87-Bev^s and U87-Bev^R generation 9 cells was done with Nestin and CD133 (stem cell markers). (**c-d**) Neurosphere formation assay revealed a much larger diameter of U87-Bev^R generation 9 neurospheres ($p=0.002$), while Bev^S cells yielded a larger number of neurospheres ($p=0.03$). (**e**) Relative distribution of Bev^S and Bev^R generation 9 neurospheres by diameter size. (**f**) Absolute cell counts from U87-Bev^S and U87-Bev^R generation 9 neurospheres. (**g**) Transcriptional analysis of prominent glioma stemness markers, GLUT3 and ZEB1, of tumor chunks from U87-Bev^S generation 9, U87-Bev^{R}1,4 and 9 reveals a positive correlation between generation number and GLUT3 and ZEB1 mRNA expression in U87-Bev^R . For ZEB1, U87-Bev^S vs U87-Bev^R generation 4 and U87-Bev^S vs U87-Bev^R

generation 9, $p<0.001$ and 0.02, respectively. For GLUT3, U87-Bev^S vs U87-Bev^R generation 4, $p=0.006$. *, $p<0.05$, **, $p<0.01$, ***, $p<0.001$. Scale bar= 100μm.

Figure 7. Increased but ineffective angiogenic gene expression in a multi-generational xenograft model of bevacizumab resistance. (**a**) The top 30 upregulated genes from the significantly enriched angiogenesis gene ontology were selected for validation by qPCR. (**b**) qPCR validation of 29 of the top 30 angiogenesis genes revealed significant overexpression of angiogenesis related genes by generation 1 of U87-Bev^R, peaking by generation 4. (**c**) Dot plots separating the PCR results for the 29 pro-angiogenic genes into 3 categories: those that were upregulated with each U87-Bev^R generation, peaking at generation 9 (left); those that peaked in U87-Bev^R generation 4 (middle); and those with no trend from generation to generation of U87-Bev^R (right). (**d**) Multiple secreted VEGF-independent pro-angiogenic factors were upregulated across U87-Bev^R generations by qPCR. (**e**) HUVEC cells on matrigel were exposed to CM from U87-Bev^S and U87-Bev^R of multiple generations in the absence and presence of bevacizumab. U87-Bev^R CM drove increased endothelial segment and mesh formation compared to U87-Bev^S conditioned media ($P=0.0007$-0.01). While bevacizumab blocked U87-Bev^S effects on HUVEC cells ($P=0.0004$), by generation nine, bevacizumab failed to block the increased U87-Bev^R effects on HUVEC cells ($P>0.05$). *, $p<0.05$, **, $p<0.01$, ***, $p<0.001$

REFERENCES

1 Ananthanarayanan B, Kim Y, Kumar S. Elucidating the mechanobiology of malignant brain tumors using a brain matrix-mimetic hyaluronic acid hydrogel platform. Biomaterials 2011; 32: 7913-7923.

2 Boisen MK, Madsen CV, Dehlendorff C, Jakobsen A, Johansen JS, Steffensen KD. The Prognostic Value of Plasma YKL-40 in Patients With Chemotherapy-Resistant Ovarian Cancer Treated With Bevacizumab. Int J Gynecol Cancer 2016; 26: 1390-1398.

3 Carbone C, Moccia T, Zhu C, Paradiso G, Budillon A, Chiao PJ *et al*. Anti-VEGF treatment-resistant pancreatic cancers secrete proinflammatory factors that contribute to malignant progression by inducing an EMT cell phenotype. Clin Cancer Res 2011; 17: 5822-5832.

4 Carbonell WS, De Lay M, Jahangiri A, Park CC, Aghi MK. β1 integrin targeting potentiates antiangiogenic therapy and inhibits the growth of bevacizumab-resistant glioblastomas. Cancer Research 2013; 73: 3145-3154.

5 Chinot OL, Wick W, Mason W, Henriksson R, Saran F, Nishikawa R *et al*. Bevacizumab plus radiotherapy-temozolomide for newly diagnosed glioblastoma. N Engl J Med 2014; 370: 709-722.

6 Clark AJ, Lamborn KR, Butowski NA, Chang SM, Prados MD, Clarke JL *et al*. Neurosurgical management and prognosis of patients with glioblastoma that progress during bevacizumab treatment. Neurosurgery 2011.

7 DeCicco-Skinner KL, Henry GH, Cataisson C, Tabib T, Gwilliam JC, Watson NJ *et al*. Endothelial cell tube formation assay for the in vitro study of angiogenesis. J Vis Exp 2014: e51312.

8 DeLay M, Jahangiri A, Carbonell WS, Hu YL, Tsao S, Tom MW *et al*. Microarray analysis verifies two distinct phenotypes of glioblastomas resistant to antiangiogenic therapy. Clin Cancer Res 2012; 18: 2930-2942.

9 Edwards LA, Li A, Berel D, Madany M, Kim NH, Liu M *et al*. ZEB1 regulates glioma stemness through LIF repression. Sci Rep 2017; 7: 69.

10 Gilbert MR, Dignam J, Won M, Blumenthal DT, Vogelbaum MA, Aldape KD *et al*. RTOG 0825: Phase III double-blind placebo-controlled trial evaluating

bevacizumab (Bev) in patients (Pts) with newly diagnosed glioblastoma (GBM). *American Society of Clinical Oncology (ASCO) annual meeting*: Chicago, 2013.

11 Jahangiri A, De Lay M, Miller LM, Carbonell WS, Hu YL, Lu K *et al*. Gene expression profile identifies tyrosine kinase c-Met as a targetable mediator of antiangiogenic therapy resistance. Clinical cancer research : an official journal of the American Association for Cancer Research 2013; 19: 1773-1783.

12 Jahangiri A, Nguyen A, Chandra A, Sidorov MK, Yagnik G, Rick J *et al*. Cross-activating c-Met/beta1 integrin complex drives metastasis and invasive resistance in cancer. Proc Natl Acad Sci U S A 2017; 114: E8685-E8694.

13 Jain RK, Duda DG, Clark JW, Loeffler JS. Lessons from phase III clinical trials on anti-VEGF therapy for cancer. Nat Clin Pract Oncol 2006; 3: 24-40.

14 Kim SS, Pirollo KF, Chang EH. Isolation and Culturing of Glioma Cancer Stem Cells. Curr Protoc Cell Biol 2015; 67: 23 10 21-10.

15 Kreisl TN, Kim L, Moore K, Duic P, Royce C, Stroud I *et al*. Phase II trial of single-agent bevacizumab followed by bevacizumab plus irinotecan at tumor progression in recurrent glioblastoma. J Clin Oncol 2009; 27: 740-745.

16 Lin JG, Kang CC, Zhou Y, Huang H, Herr AE, Kumar S. Linking invasive motility to protein expression in single tumor cells. Lab Chip 2018; 18: 371-384.

17 Masin M, Vazquez J, Rossi S, Groeneveld S, Samson N, Schwalie PC *et al*. GLUT3 is induced during epithelial-mesenchymal transition and promotes tumor cell proliferation in non-small cell lung cancer. Cancer Metab 2014; 2: 11.

18 Miller K, Wang M, Gralow J, Dickler M, Cobleigh M, Perez EA *et al*. Paclitaxel plus bevacizumab versus paclitaxel alone for metastatic breast cancer. N Engl J Med 2007; 357: 2666-2676.

19 Phillips HS, Kharbanda S, Chen R, Forrest WF, Soriano RH, Wu TD *et al*. Molecular subclasses of high-grade glioma predict prognosis, delineate a pattern of disease progression, and resemble stages in neurogenesis. Cancer cell 2006; 9: 157-173.

20 Piao Y, Liang J, Holmes L, Henry V, Sulman E, de Groot JF. Acquired resistance to anti-VEGF therapy in glioblastoma is associated with a mesenchymal transition. Clin Cancer Res 2013; 19: 4392-4403.

21 Rubenstein JL, Kim J, Ozawa T, Zhang M, Westphal M, Deen DF *et al*. Anti-VEGF antibody treatment of glioblastoma prolongs survival but results in increased vascular cooption. Neoplasia 2000; 2: 306-314.

22 Verhaak RG, Hoadley KA, Purdom E, Wang V, Qi Y, Wilkerson MD *et al*. Integrated genomic analysis identifies clinically relevant subtypes of glioblastoma characterized by abnormalities in PDGFRA, IDH1, EGFR, and NF1. Cancer cell 2010; 17: 98-110.

23 Wang R, Chadalavada K, Wilshire J, Kowalik U, Hovinga KE, Geber A *et al*. Glioblastoma stem-like cells give rise to tumour endothelium. Nature 2010; 468: 829-833.

24 Wen PY, Prados M, Chamberlain M, Cloughesy TF, Drappatz J, Mikkelsen T *et al*. A Phase 2 Study of XL184, an Inhibitor of Met, VEGFR2, and RET, in patients with progressive glioblastoma multforme. *Society for Neuro-Oncology Annual Meeting*: New Orleans, LA, 2009.

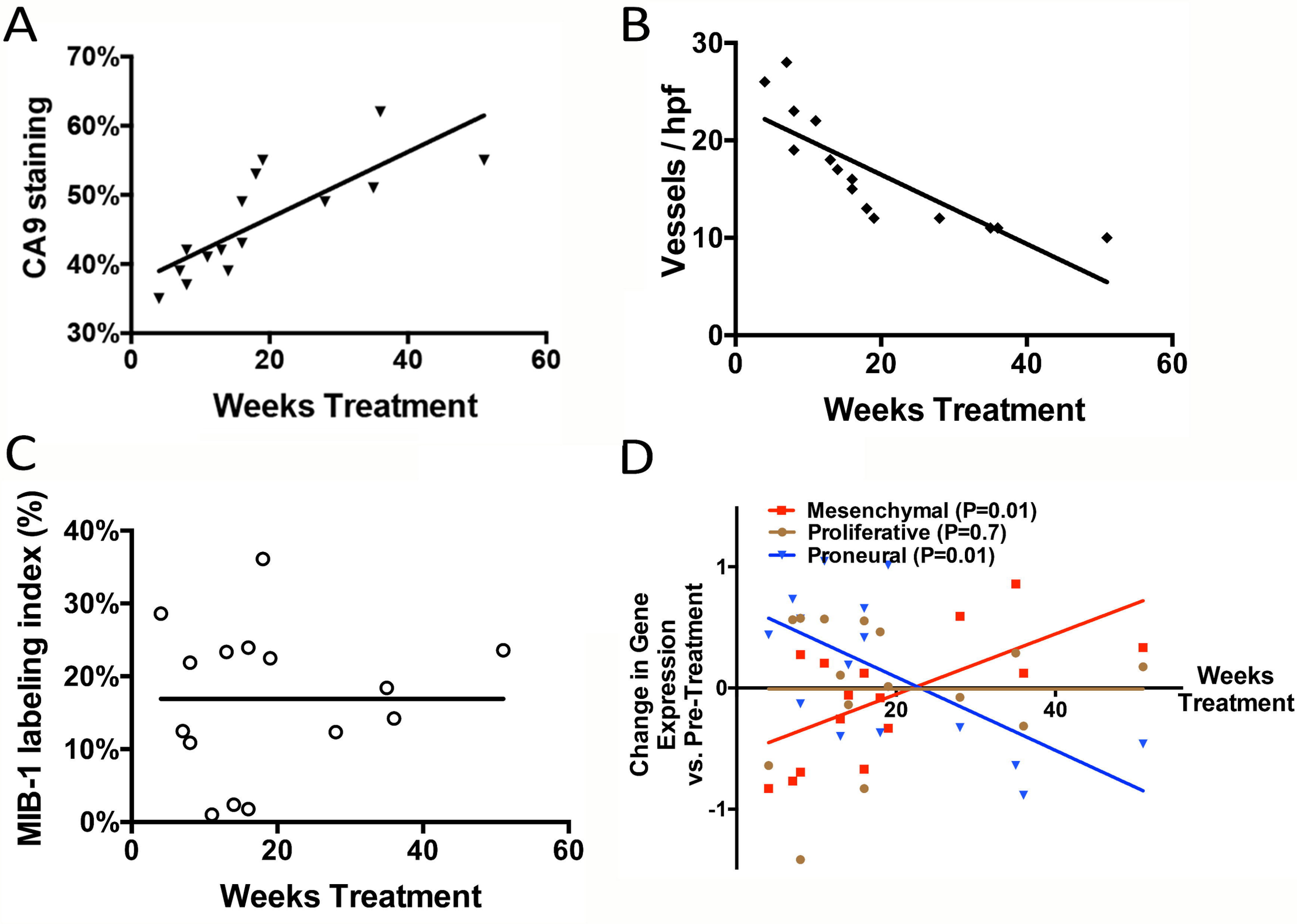
A
CA9 staining
70%
60%
50%
40%
30%
0
20
40
60
Weeks Treatment
B
Vessels / hpf
30
20
10
0
0
20
40
60
Weeks Treatment
C
MIB-1 labeling index (%)
40%
30%
20%
10%
0%
0
20
40
60
Weeks Treatment
D
Mesenchymal (P=0.01)
Proliferative (P=0.7)
Proneural (P=0.01)
Change in Gene Expression vs. Pre-Treatment
1
0
-1
20
40
Weeks Treatment

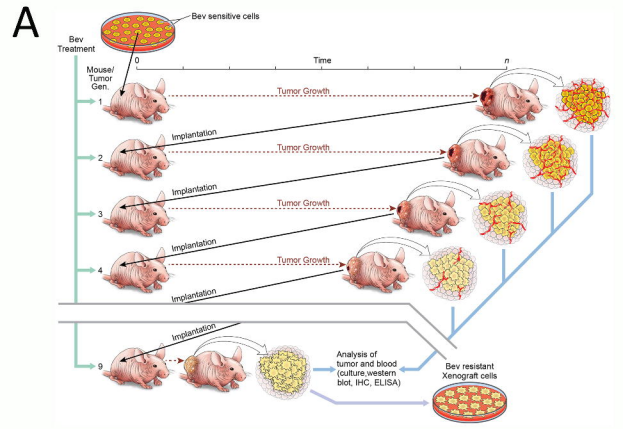
A
Bev sensitive cells
Bev Treatment
Mouse/ Tumor Gen.
Time
0
n
1
2
3
4
9
Tumor Growth
Implantation
Analysis of tumor and blood (culture,western blot, IHC, ELISA)
Bev resistant Xenograft cells

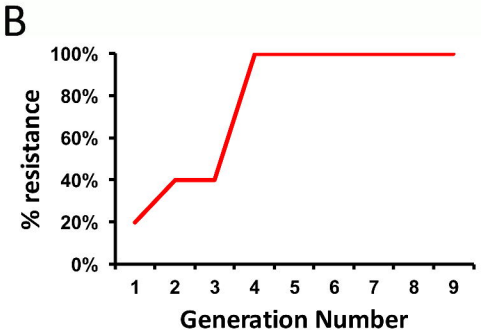
B
% resistance
100%
80%
60%
40%
20%
0%
1 2 3 4 5 6 7 8 9
Generation Number

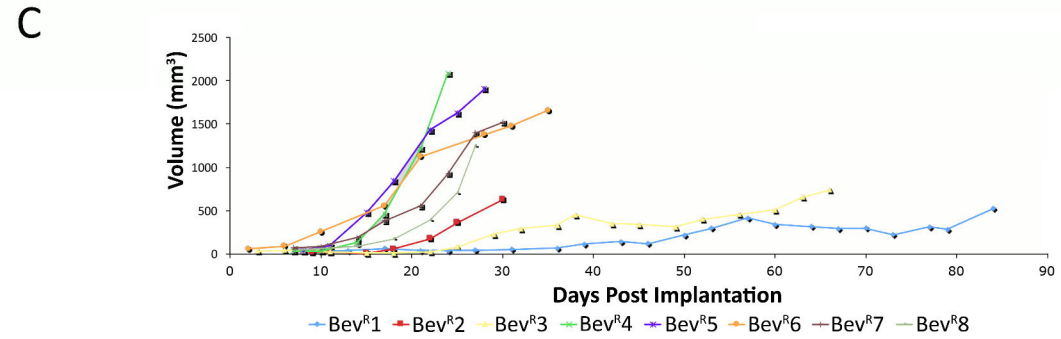
C
Volume (mm³)
2500
2000
1500
1000
500
0
0 10 20 30 40 50 60 70 80 90
Days Post Implantation
BevR1 BevR2 BevR3 BevR4 BevR5 BevR6 BevR7 BevR8

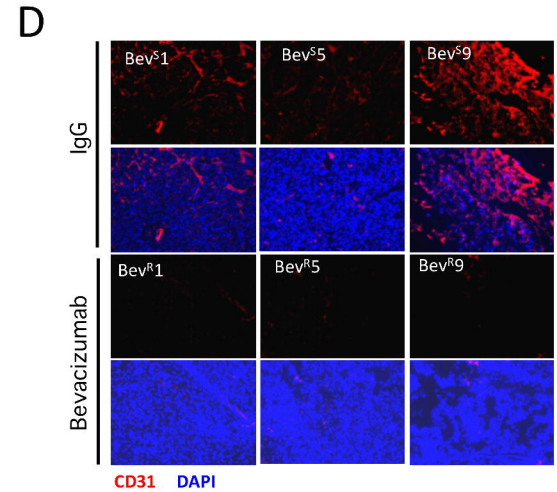
D
IgG
Bevacizumab
BevS1
BevS5
BevS9
BevR1
BevR5
BevR9
CD31 DAPI

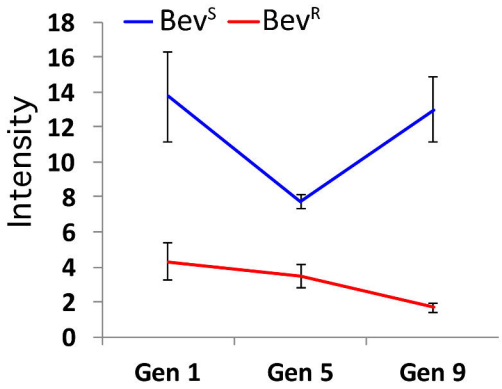
BevS BevR
Intensity
18
16
14
12
10
8
6
4
2
0
Gen 1 Gen 5 Gen 9

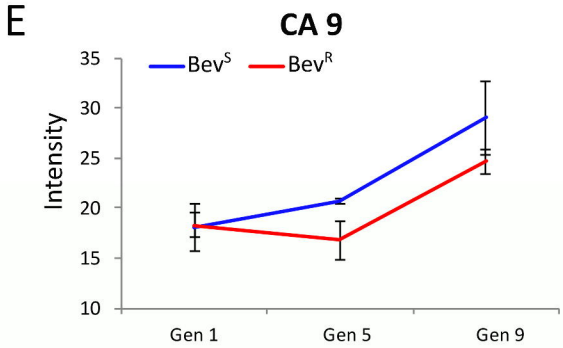
E
CA 9
BevS BevR
Intensity
35
30
25
20
15
10
Gen 1 Gen 5 Gen 9

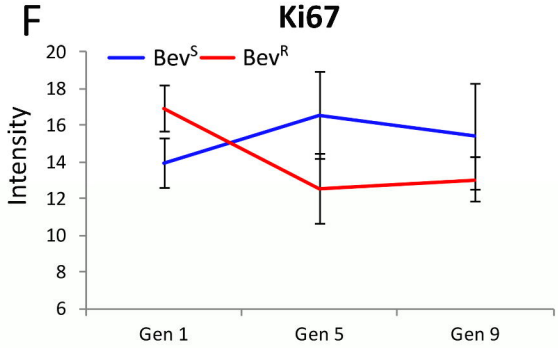
F
Ki67
BevS BevR
Intensity
20
18
16
14
12
10
8
6
Gen 1 Gen 5 Gen 9

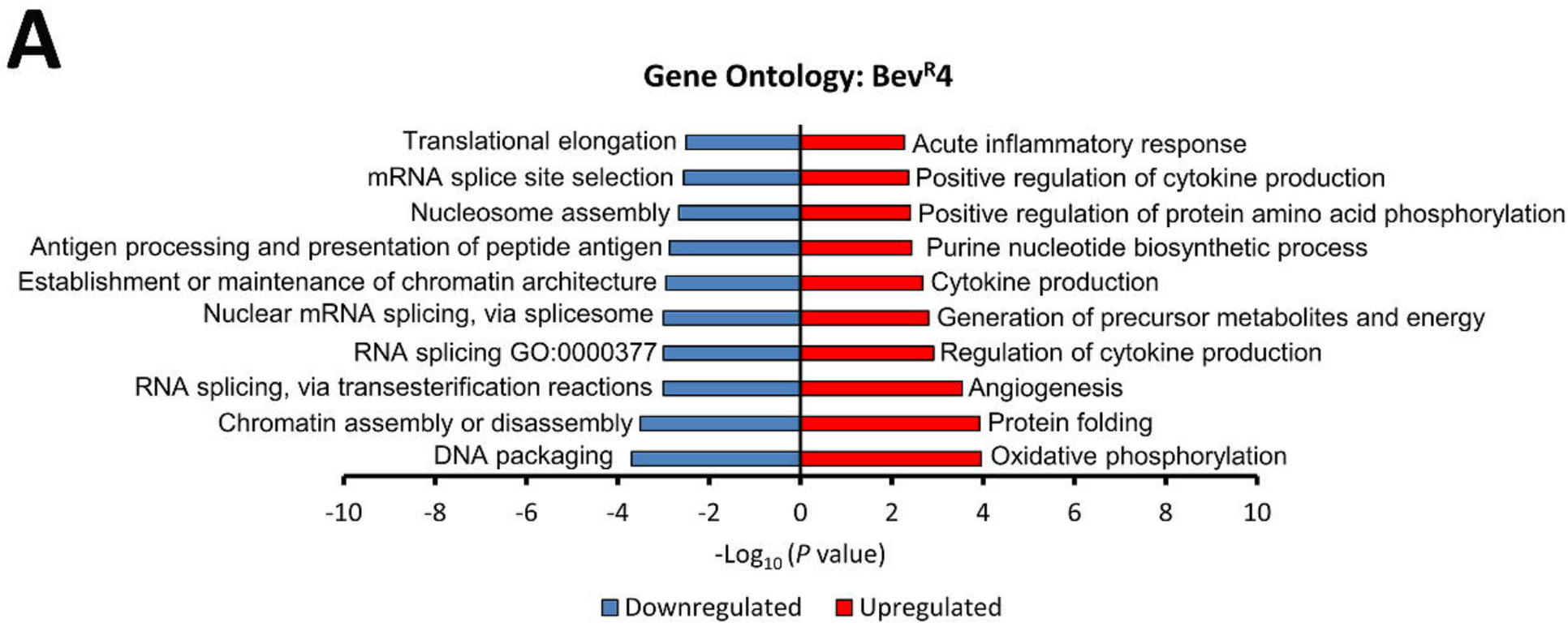
A
Gene Ontology: Bev^R4
Translational elongation
mRNA splice site selection
Nucleosome assembly
Antigen processing and presentation of peptide antigen
Establishment or maintenance of chromatin architecture
Nuclear mRNA splicing, via splicesome
RNA splicing GO:0000377
RNA splicing, via transesterification reactions
Chromatin assembly or disassembly
DNA packaging
Acute inflammatory response
Positive regulation of cytokine production
Positive regulation of protein amino acid phosphorylation
Purine nucleotide biosynthetic process
Cytokine production
Generation of precursor metabolites and energy
Regulation of cytokine production
Angiogenesis
Protein folding
Oxidative phosphorylation
-10 -8 -6 -4 -2 0 2 4 6 8 10
-Log10 (P value)
Downregulated
Upregulated

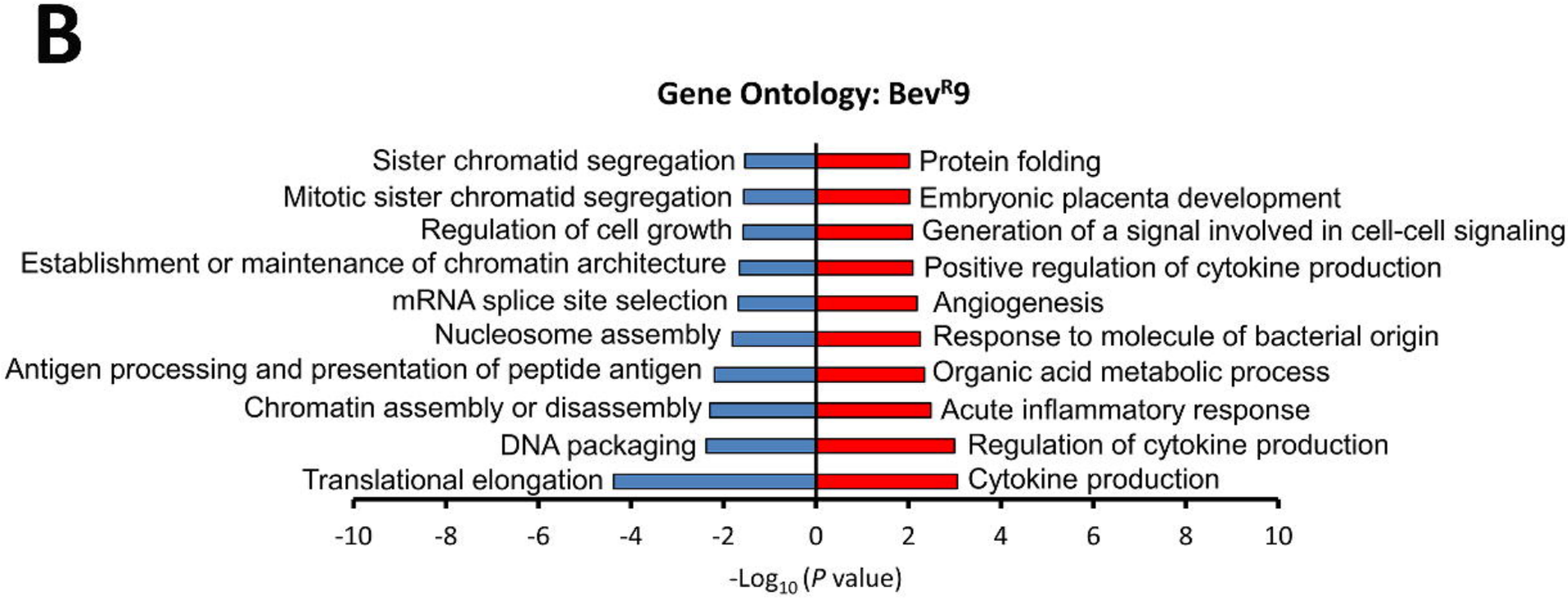
B
Gene Ontology: Bev^R9
Sister chromatid segregation
Mitotic sister chromatid segregation
Regulation of cell growth
Establishment or maintenance of chromatin architecture
mRNA splice site selection
Nucleosome assembly
Antigen processing and presentation of peptide antigen
Chromatin assembly or disassembly
DNA packaging
Translational elongation
Protein folding
Embryonic placenta development
Generation of a signal involved in cell-cell signaling
Positive regulation of cytokine production
Angiogenesis
Response to molecule of bacterial origin
Organic acid metabolic process
Acute inflammatory response
Regulation of cytokine production
Cytokine production
-10 -8 -6 -4 -2 0 2 4 6 8 10
-Log10 (P value)

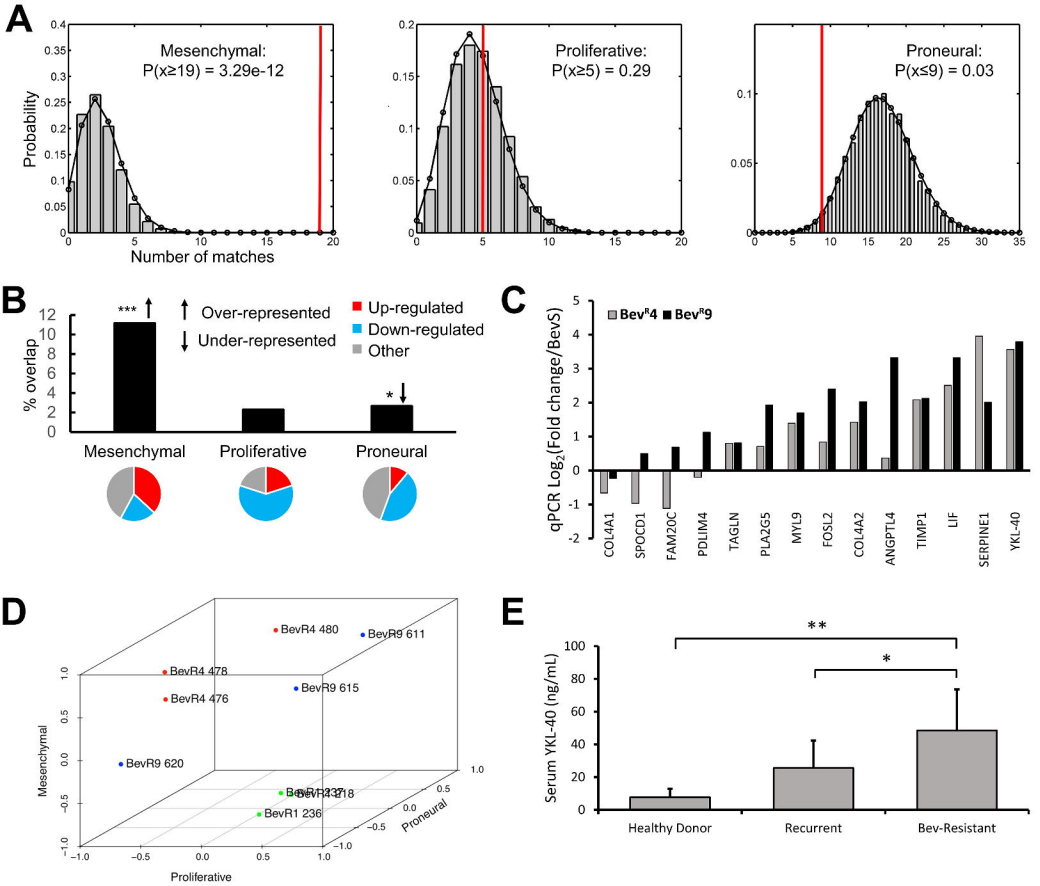
A
Mesenchymal:
P(x≥19) = 3.29e-12
Proliferative:
P(x≥5) = 0.29
Proneural:
P(x≤9) = 0.03
Probability
Number of matches
B
Over-represented
Under-represented
Up-regulated
Down-regulated
Other
% overlap
Mesenchymal
Proliferative
Proneural
C
BevR4
BevR9
qPCR Log2(Fold change/BevS)
COL4A1
SPOCD1
FAM20C
PDLIM4
TAGLN
PLA2G5
MYL9
FOSL2
COL4A2
ANGPTL4
TIMP1
LIF
SERPINE1
YKL-40
D
BevR4 480
BevR9 611
BevR4 478
BevR9 615
BevR4 476
BevR9 620
BevR1 236
Mesenchymal
Proliferative
Proneural
E
Serum YKL-40 (ng/mL)
Healthy Donor
Recurrent
Bev-Resistant

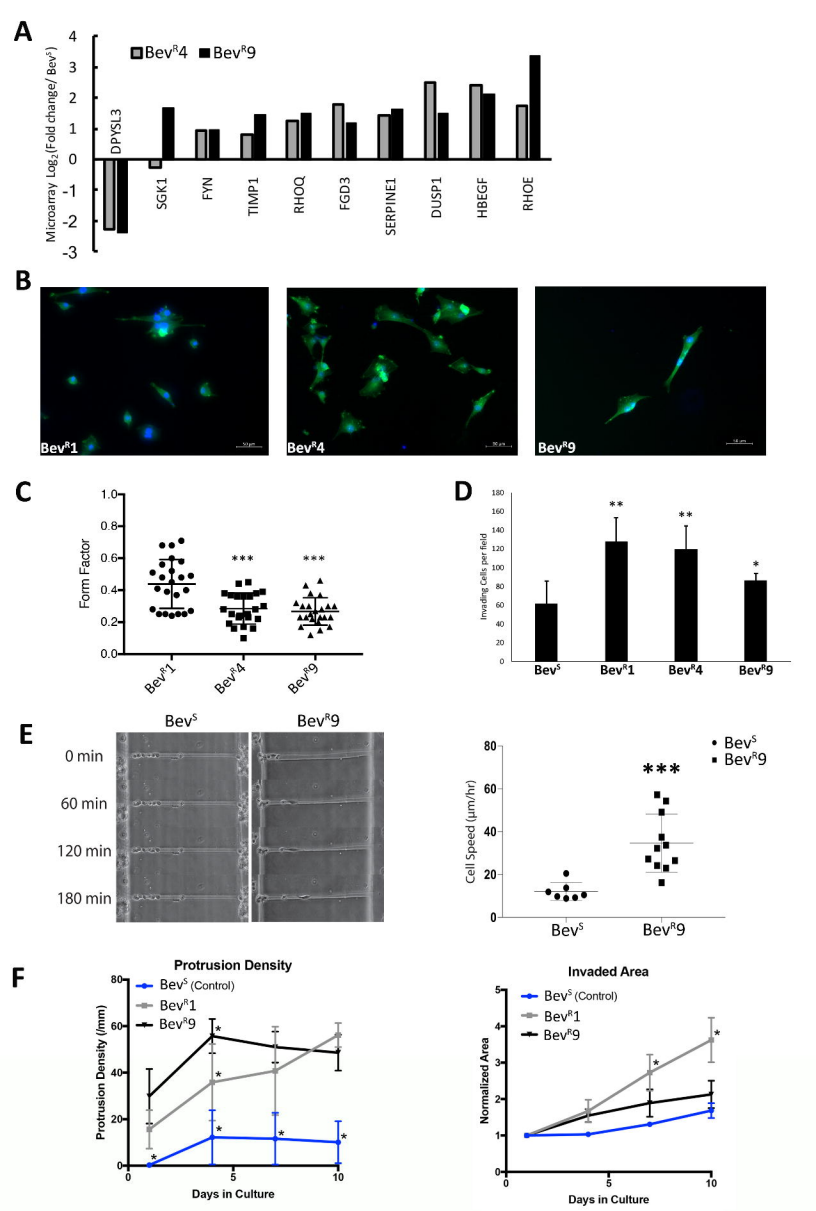
A
Bev^{R}4
Bev^{R}9
Microarray Log$_2$(Fold change/ Bev^S)
DPYSL3
SGK1
FYN
TIMP1
RHOQ
FGD3
SERPINE1
DUSP1
HBEGF
RHOE
B
Bev^{R}1
Bev^{R}4
Bev^{R}9
C
Form Factor
Bev^{R}1
Bev^{R}4
Bev^{R}9
D
Invading Cells per field
Bev^S
Bev^{R}1
Bev^{R}4
Bev^{R}9
E
Bev^S
Bev^{R}9
0 min
60 min
120 min
180 min
Cell Speed (µm/hr)
Bev^S
Bev^{R}9
F
Protrusion Density
Bev^S (Control)
Bev^{R}1
Bev^{R}9
Protrusion Density (/mm)
Days in Culture
Invaded Area
Bev^S (Control)
Bev^{R}1
Bev^{R}9
Normalized Area
Days in Culture

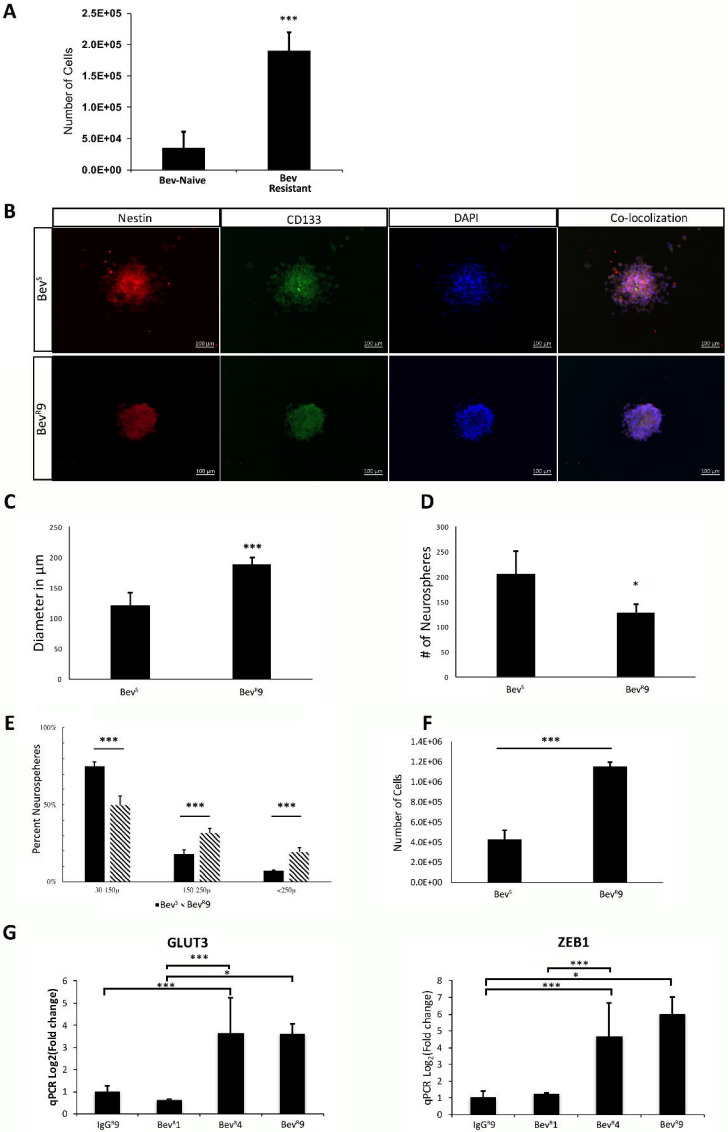
A
Number of Cells
2.5E+05
2.0E+05
1.5E+05
1.0E+05
5.0E+04
0.0E+00
***
Bev-Naive
Bev Resistant
B
Nestin
CD133
DAPI
Co-locolization
Bev^S
Bev^{R}9
100 µm
C
Diameter in µm
250
200
150
100
50
0
***
Bev^S
Bev^{R}9
D
# of Neurospheres
300
250
200
150
100
50
0
*
Bev^S
Bev^{R}9
E
Percent Neurospeheres
100%
50%
0%
***
***
***
30-150µ
150-250µ
<250µ
Bev^S
Bev^{R}9
F
Number of Cells
1.4E+06
1.2E+06
1.0E+06
8.0E+05
6.0E+05
4.0E+05
2.0E+05
0.0E+00
***
Bev^S
Bev^{R}9
G
GLUT3
qPCR Log2(Fold change)
6
5
4
3
2
1
0
***
*
***
IgG^{R}9
Bev^{R}1
Bev^{R}4
Bev^{R}9
ZEB1
qPCR Log2(Fold change)
8
7
6
5
4
3
2
1
0
***
*
***
IgG^{R}9
Bev^{R}1
Bev^{R}4
Bev^{R}9

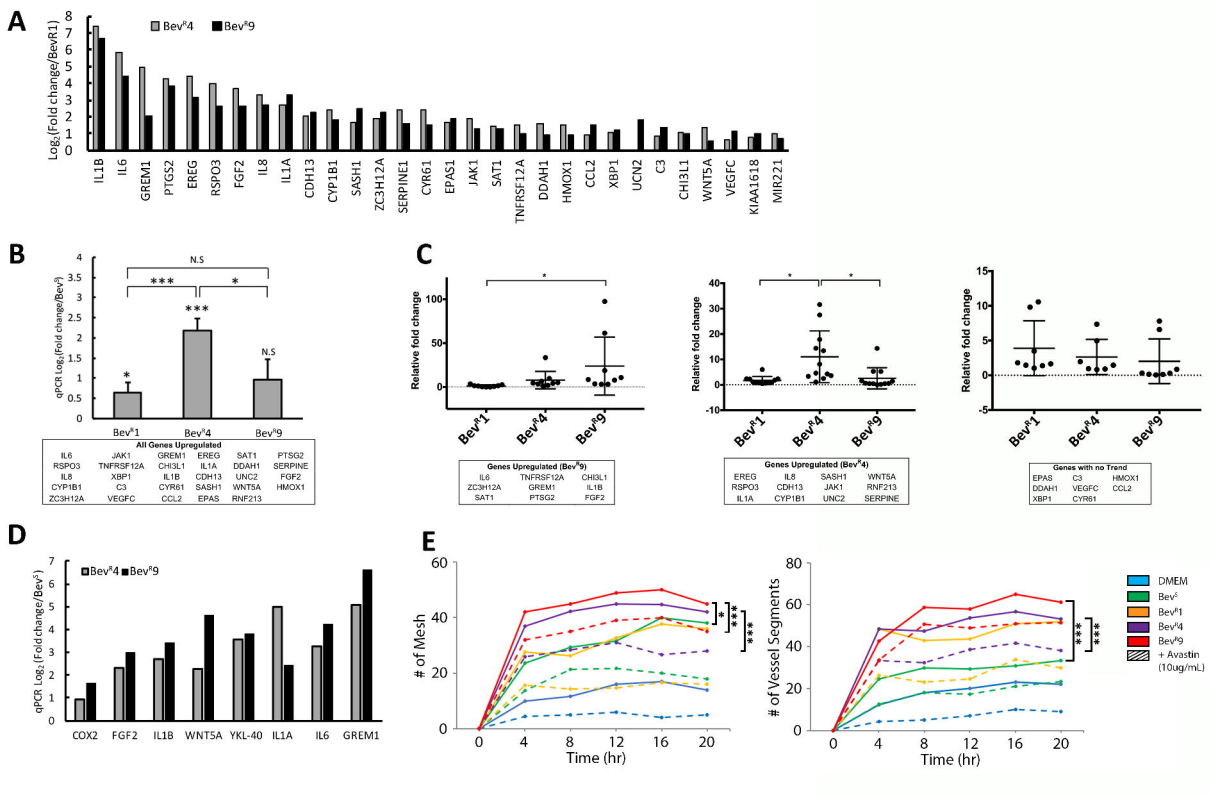
A
Bev^{R}4
Bev^{R}9
Log$_2$(Fold change/BevR1)
IL1B
IL6
GREM1
PTGS2
EREG
RSPO3
FGF2
IL8
IL1A
CDH13
CYP1B1
SASH1
ZC3H12A
SERPINE1
CYR61
EPAS1
JAK1
SAT1
TNFRSF12A
DDAH1
HMOX1
CCL2
XBP1
UCN2
C3
CHI3L1
WNT5A
VEGFC
KIAA1618
MIR221
B
qPCR Log$_2$(Fold change/Bev^S)
N.S
***
*
Bev^{R}1
Bev^{R}4
Bev^{R}9
All Genes Upregulated
IL6 JAK1 GREM1 EREG SAT1 PTSG2
RSPO3 TNFRSF12A CHI3L1 IL1A DDAH1 SERPINE
IL8 XBP1 IL1B CDH13 UNC2 FGF2
CYP1B1 C3 CYR61 SASH1 WNT5A HMOX1
ZC3H12A VEGFC CCL2 EPAS RNF213
C
Relative fold change
Genes Upregulated (Bev^{R}9)
IL6 TNFRSF12A CHI3L1
ZC3H12A GREM1 IL1B
SAT1 PTSG2 FGF2
Genes Upregulated (Bev^{R}4)
EREG IL8 SASH1 WNT5A
RSPO3 CDH13 JAK1 RNF213
IL1A CYP1B1 UNC2 SERPINE
Genes with no Trend
EPAS C3 HMOX1
DDAH1 VEGFC CCL2
XBP1 CYR61
D
Bev^{R}4
Bev^{R}9
qPCR Log$_2$ (Fold change/Bev^S)
COX2
FGF2
IL1B
WNT5A
YKL-40
IL1A
IL6
GREM1
E
# of Mesh
# of Vessel Segments
Time (hr)
DMEM
Bev^S
Bev^{R}1
Bev^{R}4
Bev^{R}9
+ Avastin (10ug/mL)